CHIN. PHYS. LETT. Vol. 32, No. 2 (2015) 024205

Synthesis and Optical Responses of Ag@Au/Ag@Au Double Shells *

LI Ying-Ying(李颖颖), LIU Xiao-Li(刘晓丽), YANG Da-Jie(杨大杰),
HAO Zhong-Hua(郝中华)**, WANG Qu-Quan(王取泉)**

Key Laboratory of Artificial Micro- and Nano-structures (Ministry of Education), and School of Physics and Technology, Wuhan University, Wuhan 430072

(Received 30 September 2014)

We synthesize hollow-structured Ag@Au nanoparticles with single porous shell and Ag@Au/Ag@Au double shells by using the galvanic replacement reaction and investigate their linear and nonlinear optical properties. Our results show that the surface plasmon resonance wavelength of the hollow porous nanoparticles could be easily tuned in a wide range in the visible and near infrared region by controlling the volume of $HAuCl_4$. The nonlinear optical refraction of the double-shelled Ag@Au/Ag@Au nanoparticles is prominently enhanced by the plasmon resonance. Our findings may find applications in biosensors and nonlinear optical nanodevices.

PACS: 42.65.−k, 52.25.−b, 78.40.−q, 78.67.Rb DOI: 10.1088/0256-307X/32/2/024205

Noble metal (such as gold and silver) nanoparticles (NPs) have been a research focus in recent years because of their unique optical properties induced by surface plasmon resonance (SPR) and wide applications in the field of catalysis, photonics, electronics, biological sensing, surface enhanced Raman scattering (SERS), and nonlinear optical devices.[1−5] The plasmon resonance frequency mainly depends on the compositions, structures, dimensions and morphologies of the nanostructures, which could be easily tuned in the visible-to-near-infrared (NIR) region. Among the noble metal NPs with SPR effect, the hollow nanostructures have strong SPR, and the corresponding resonance wavelength can be easily tuned by varying the dimensions of the core and the shell.[5−13]

Various types of hollow metal nanostructures have been investigated, such as cubic nanoboxes,[14−16,20] nanocages,[8,9,17,18] prism-shaped nanoboxes,[19,20] triangular nanorings,[19−21] nanoshells and nanotubes,[22−24] and multi-layer composite nanoparticles.[1,25−27] Xia *et al.* have developed various hollow nanostructures of Ag, Au, Pt, and Pd with controlled pore volume and wall thickness via the galvanic replacement reaction and have investigated their applications, such as biomedical sensing and imaging, catalysis, and SERS.[9,13,19,28,29] The enhancement of nonlinear optical properties of such multishelled hollow structures is expected but has seldom been reported.

In the present study, we synthesize hollow-structured Ag@Au NPs with single and Ag@Au/Ag@Au NPs with double porous shells by using the galvanic replacement reaction between the Ag NPs and aqueous $HAuCl_4$ solution. We also investigate the extinction properties of the four samples with different structures in the synthesis process, and compared the nonlinear optical refraction properties of the single-shelled Ag@Au NPs and double-shelled Ag@Au/Ag@Au NPs. The larger local field enhancement in the double-shelled nanostructures is further revealed by measuring the nonlinear optical refraction coefficient.

Ag NPs were synthesized by reducing $AgNO_3$ with ethylene glycol (EG) in the presence of ploy vinyl pyrrolidone (PVP),[13,28] in which $AgNO_3$ as a precursor to elemental Ag, EG as both solvent and reducing agent, and PVP as a capping reagent and colloidal stabilizer. In a typical synthesis of quasi-spherical Ag NPs, 2.5 mL EG solution of $AgNO_3$ (0.16 M) and 5 mL EG solution of PVP (0.34 M) were simultaneously added to 5 mL EG heated in a 50 mL round-bottom flask at 155℃ with magnetic stirring. The following procedures to synthesize Ag@Au NPs with single shells and Ag@Au/Ag@Au NPs with double shells by the galvanic replacement reaction between Ag and aqueous $HAuCl_4$ solution were similar to the method reported in Refs. [26,29].

The extinction spectra of the samples in different growth steps were measured by using a Varian Cary 5000 spectrometer. The transmission electron microscopy (TEM) images of the metal nanoparticles were taken on a JEOL (2010 HT, at 200 kV), and EDX was performed on an EDAX equipped on an FEG SEM Sirion 200 operated at an accelerating voltage of 20.0 kV. Nonlinear absorption (NLA) and nonlinear refraction (NLR) were investigated by the open- and closed-aperture Z-scan techniques.[30−33] The ultrafast laser pulses used in *Z*-scan measurements were generated by a wavelength-tunable Ti/Sapphire mode-locked laser (Mira 900, Coherent) with a pulse width of 100 fs and a repetition rate of 76 MHz.

Figure 1(a) shows a schematic illustration of the

*Supported by the National Natural Science Foundation of China under Grant Nos 11174229, 11204221 and 11374236, and the National Basic Research Program of China under Grant No 2011CB922201.

**Corresponding author. Email: qqwang@whu.edu.cn; zhhao@whu.edu.cn

© 2015 Chinese Physical Society and IOP Publishing Ltd

procedures for preparing the double-shelled hollow Ag@Au/Ag@Au NPs. Firstly, quasi-spherical Ag NPs are synthesized. Secondly, hollow nanostructures consisting of Au and Ag alloy are obtained by the galvanic replacement reaction, which is labeled as Ag@Au NPs. Thirdly, another Ag layer is deposited onto the as-prepared Ag@Au NPs (labeled as Ag@Au/Ag NPs). Finally, by using galvanic replacement reaction between the outer Ag layer and aqueous $HAuCl_4$ solution, the double nanoshells are obtained (labeled as Ag@Au/Ag@Au NPs). Figures 1(b)–1(e) give the TEM images of the morphological and structural changes of the hollow porous shelled NPs corresponding to the four growth steps illustrated in Fig. 1(a). One can see that the diameters of the as-synthesized NPs in the four steps are approximately 70, 100, 100–110 and 120 nm, respectively. Figure 1(f) shows the corresponding EDX spectra of the four NPs. One can clearly see that the relative signal intensities of Au and Ag for the various structures of our samples are different.

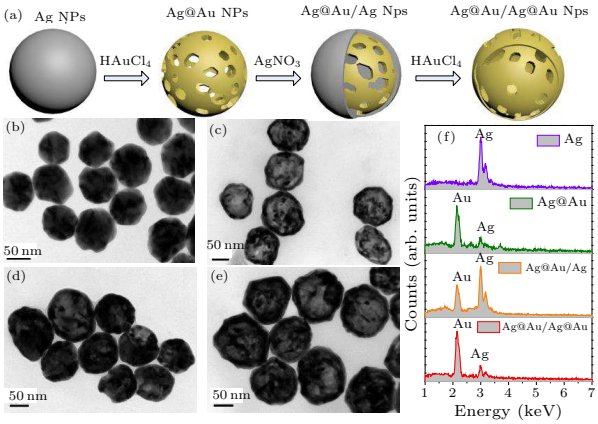


Fig. 1. (a) Schematic illustration of the procedures to grow the double-shelled hollow Ag@Au/Ag@Au NPs. TEM images of the as-prepared Ag NPs (b), hollow porous Ag@Au NPs (c), Ag@Au/Ag NPs (d), and double porous shelled Ag@Au/Ag@Au NPs (e). The scale bar is 50 nm. (f) The corresponding EDX spectra of the four samples.

We then experimentally and theoretically study the extinction properties of the products at different growth steps. Figures 2(a)–2(c) are the experimental results and Figs. 2(d)–2(f) are the simulated ones. Firstly, the sacrificial template Ag NPs with SPR peak of ∼420 nm (grey line in Fig. 2(a)) is synthesized, and then the galvanic replacement reaction between Ag NPs and $HAuCl_4$ solution takes place after different volumes of $HAuCl_4$ solution are added.[8,13,28] As shown in Fig. 2(a), when the adding volume of $HAuCl_4$ aqueous solution increases from 4 mL to 11 mL, the SPR peak of Ag NPs almost disappears and the main SPR peak of the alloy Ag@Au NPs shifts red from 700 nm to 910 nm. This means that Ag@Au alloy NPs were formed by the consumption of Ag during the deposition of Au on the surface of Ag NPs.[34–36] Moreover, this shift of peak position could be ascribed to the increase of hollow void size and the thinning of the shell walls, and the formation of pinholes in the shell walls may also be involved.[28] In the third step, another layer of Ag grows on the as-prepared Ag@Au NPs by adding $AgNO_3$ into aqueous suspensions. The normalized extinction spectra of the obtained Ag@Au/Ag NPs with different volumes of $AgNO_3$ are presented in Fig. 2(b). As the adding volume of $AgNO_3$ increases from 0.1 to 1.0 mL, the main SPR peak of Ag@Au/Ag NPs shifts blue from ∼665 nm to ∼460 nm. The blue shift of the main SPR peak is caused by the dipole mode of Ag@Au/Ag NPs with the increasing thickness of Ag. Similarly, when preparing Ag@Au/Ag@Au NPs, we observe that the SPR peak shifts red from 666 nm to 734 nm with different volumes of $HAuCl_4$ solution added.

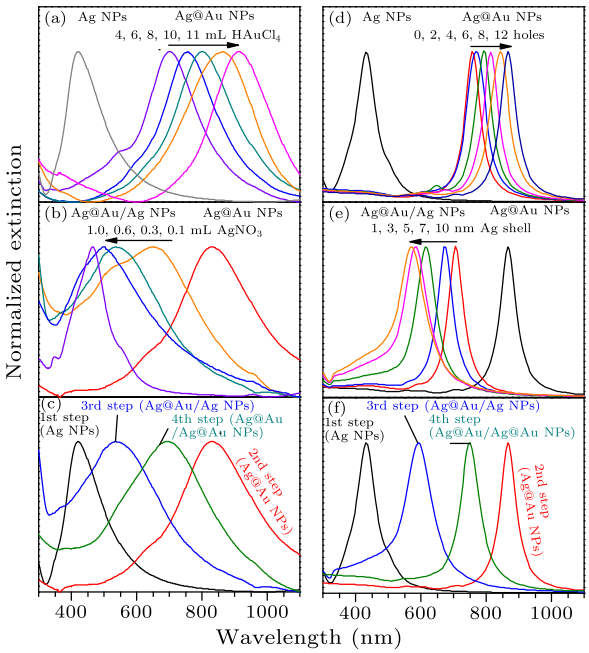


Fig. 2. Normalized experimental (left panel) and simulated (right panel) extinction spectra of the samples for (a) and (d) Ag NPs and Ag@Au NPs with different volumes of $HAuCl_4$, (b) and (e) Ag@Au/Ag NPs with different volumes of $AgNO_3$, and (c) and (f) the four samples (Ag, Ag@Au, Ag@Au/Ag, and Ag@Au/Ag@Au) corresponding to the four steps in the synthesis procedure. The simulated extinction curves agree well with the experimental results.

As presented in Fig. 2(c), the normalized extinction spectra of the four samples with different structures in the four synthesis steps demonstrate that the corresponding SPR wavelength varies in a wide range. The SPR wavelength of the initial Ag NPs is at 420 nm. After the first Au nanoshell is formed, the SPR peak of Ag@Au NPs red shifts to 830 nm. As the second Ag layer is deposited on the surface of Ag@Au NPs, the SPR peak of Ag@Au/Ag NPs shifts back to 520 nm. Along with the replacement reaction, the consumption of the second layer of Ag leads to the formation of Ag@Au/Ag@Au double-shelled NPs and

the corresponding SPR peak shifts to 700 nm.

To explore the nature of the SPR peak shift and electric field distribution at different growth steps, the finite difference time domain (FDTD) simulation is performed. We design four models corresponding to the NPs in Fig. 1(a), the shapes and dimensions are chosen according to the TEM images. The refractive indexes of Au and Ag are taken from Refs. [37,38], respectively. Circularly polarized light is used for simulating the source. Figures 2(d)–2(f) are the simulation curves of the normalized extinction spectra corresponding to our experimental results of Figs. 2(a)–2(c), respectively. The number of holes in the simulation corresponds to the volume of $HAuCl_4$ aqueous solution, and the thickness of the Ag shell corresponds to the volume of $AgNO_3$. One can see that the theoretical results agree well with our experimental results. The changes of structures and component that result in the peak shift of SPR. The experimental SPR peaks being broader than the theoretical peaks originate from the inhomogeneous morphologies of the samples.

Figure 3 shows the electric field distribution of the four NPs simulated by the FDTD method. The maximum values are 50, 300, 50 and 150, respectively. It can be seen that large field enhancement takes place at the surface of the NPs and around the holes. For the double shelled Ag@Au/Ag@Au NPs, the great field enhancement is also demonstrated in the gap between the two nanoshells.

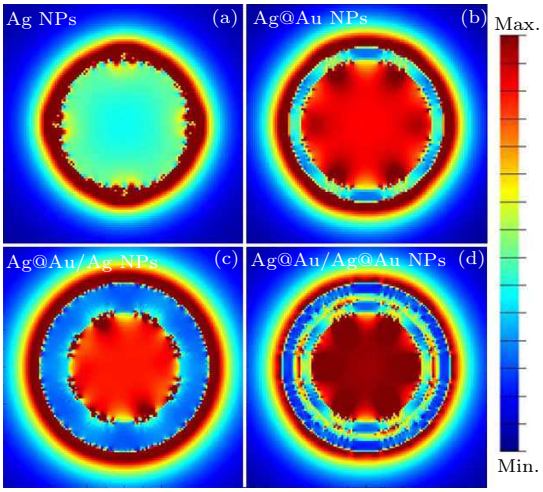


Fig. 3. FDTD simulated electric field distribution of the four samples, Ag NPs, Ag@Au NPs, Ag@Au/Ag NPs and Ag@Au/Ag@Au NPs under their resonant excitation.

To investigate the average local field enhancements of such double-shelled Ag@Au/Ag@Au NPs and single-shelled Ag@Au NPs, we further carry out the measurement of third-order optical nonlinearity. The closed-aperture Z-scan results normalized by the corresponding open aperture transmittance ($T_{\rm CL}/T_{\rm OP}$) of single shelled Ag@Au NPs ($\lambda_{\rm SPR}$ = 816 nm) and three double shelled Ag@Au/Ag@Au NPs ($\lambda_{\rm SPR}$ = 696, 704 and 728 nm) are shown in Fig. 4. The excitation wavelengths are chosen to be resonant with their SPR wavelengths. The theoretical relationship of $T_{\rm CL}/T_{\rm OP}$ is expressed as[32]

$$\frac{T_{\rm CL}(Z)}{T_{\rm OP}(Z)} = 1 + \frac{4\Delta\phi_0 Z/Z_0}{((Z/Z_0)^2+9)((Z/Z_0)^2+1)},$$

where $\Delta\phi_0$ is related to the nonlinear refractive coefficient γ by $\Delta\phi_0 = \gamma k I_0 L_{\rm eff}$, I_0 is the peak irradiance at the focus (z=0), $L_{\rm eff}$ is the effective thickness of samples, $k = 2\pi/\lambda$ is the wave vector of the laser beam, and z_0 is the Rayleigh length of the Gaussian incident beam. The nonlinear refractive coefficient γ is calculated to be -0.31×10^{-4} cm^2/GW for Ag@Au NPs with single shell. The γ values of the three double shelled Ag@Au/Ag@Au NPs are -0.15×10^{-4}, -0.33×10^{-4} and -0.51×10^{-4} cm^2/GW, respectively, and the increasing absolute values of γ for double shelled NPs are ascribed to the increase of the content of gold accompanied with the loss of silver content on the outer shell. When the volume of $HAuCl_4$ is added to a certain extent, holes might form in the shell by the galvanic replacement reaction, which can greatly enhance the local field and result in the larger nonlinear refraction coefficient. It is to be noted that in our experiment the measured nonlinear optical signal is the average effect of the NPs and the field enhancement effect of the double shelled NPs would be decreased for the inhomogeneous morphology of the synthesized NPs. SERS measurement might be a more powerful tool to reflect the local field enhancement of the hollow porous double-shelled Ag@Au/Ag@Au NPs when the molecules are located in the 'hot spots', which is further to be carried out.

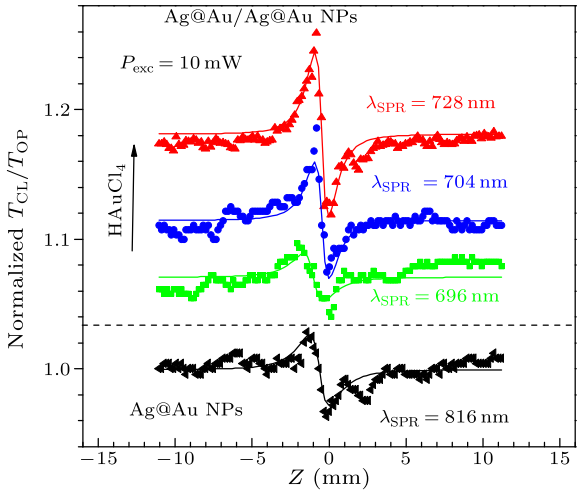


Fig. 4. The closed-aperture Z-scan nonlinear transmittance of single-shelled Ag@Au NPs and double-shelled Ag@Au/Ag@Au NPs with different SPR peaks by adding different volumes of $HAuCl_4$. The curves are shifted vertically for clear presentation.

In conclusion, we have synthesized hollow-structured Ag@Au and Ag@Au/Ag@Au NPs with sin-

gle and double shells by using the galvanic replacement reaction, and have investigated their linear and nonlinear optical properties. Our results show that the surface plasmon resonance wavelength of the hollow NPs could be easily tuned ranging from visible to NIR region by controlling the volume of the $HAuCl_4$. Compared with the hollow-structured Ag@Au NPs with single shell, the nonlinear optical refraction efficient of the double-shelled Ag@Au/Ag@Au NPs is prominently enhanced, which is attributed to field enhancement induced by the SPR between the two porous shells. Due to the NIR absorption and the local field enhancement, the Au/Ag alloyed hollow nanostructures in this study may have potential applications in biosensing and designing of optical nanodevices.

We thank F. Nan for Z-scan measurements and Q. Fu for providing support of EDX.

References

[1] Long H et al 2008 *Chin. Phys. Lett.* **25** 4135
[2] Xue J C et al 2013 *Nanoscale Res. Lett.* **8** 295
[3] Kim K, Kim K L and Lee S J 1976 *Chem. Phys. Lett.* **43** 77
[4] Haes A J and Van Duyne R P 2002 *J. Am. Chem. Soc.* **124** 10596
[5] Sun X F and Wang L X 2014 *Acta Phys. Sin.* **63** 097301 (in Chinese)
[6] Ren M L et al 2013 *Chin. Phys. Lett.* **30** 097301
[7] Philip R et al 2000 *Phys. Rev.* B **62** 13160
[8] Zhou L et al 2008 *Chin. Phys. Lett.* **25** 1776
[9] Chen J Y et al 2005 *Nano Lett.* **5** 473
[10] Vongsavat V et al 2011 *ACS Appl. Mater. Interfaces* **3** 3616
[11] Jain P K and El-Sayed M A 2007 *J. Phys. Chem.* C **111** 17451
[12] Liang H P et al 2005 *J. Phys. Chem.* B **109** 7795
[13] Sun Y G and Xia Y N 2002 *Anal. Chem.* **74** 5297
[14] Wang W Z et al 2005 *Adv. Mater.* **17** 2110
[15] Peng Z M et al 2010 *Nano Lett.* **10** 1492
[16] Cao M, Wang M and Gu N 2009 *J. Phys. Chem.* C **113** 1217
[17] Mahmoud M A, Saira F and El-Sayed M A 2010 *Nano Lett.* **10** 3764
[18] Cao H L et al 2005 *J. Am. Chem. Soc.* **127** 16024
[19] Sun Y G and Xia Y N 2003 *Adv. Mater.* **15** 695
[20] Aherne D et al 2010 *Adv. Funct. Mater.* **20** 1329
[21] Xin G Q et al 2009 *Cryst. Growth Des.*. **9** 2008 2012
[22] Liu L, Yoo S H and Park S 2010 *Chem. Mater.* **22** 2681
[23] Dong W et al 2006 *Adv. Mater.* **18** 755
[24] Park J H, Oh S G and Jo B W 2004 *Mater. Chem. Phys.* **87** 301
[25] Beyene H T et al 2011 *Plasmonics* **6** 255
[26] Hong S et al 2014 *Chem. Mater.* **26** 3618
[27] Ma Y W et al 2010 *Chin. Phys. Lett.* **27** 064204
[28] Sun Y G and Xia Y N 2003 *Nano Lett.* **3** 1569
[29] Ma Y Y et al 2010 *ACS Nano* **4** 6725
[30] Gong H M et al 2007 *Chin. Phys. Lett.* **24** 3443
[31] Wang Q Q et al 2006 *Adv. Funct. Mater.* **16** 2405
[32] Sheik-Bahae M et al 1990 *IEEE J. Quantum Electron.* **26** 760
[33] Chen D J et al 2005 *Chin. Phys. Lett.* **22** 2286
[34] Zhu J 2005 *Physica* E **27** 296
[35] Mallin M P and Murphy C J 2002 *Nano Lett.* **2** 1235
[36] Yang J, Lee J Y and Too H P 2005 *J. Phys. Chem.* B **109** 19208
[37] Johnson P B and Christy R W 1972 *Phys. Rev.* B **6** 4370
[38] Palik E D 1985 *Handbook of Optical Constants of Solids* (New York: Academic Press) p 350